Custom Beam Shaping for High-Power Fiber Laser Welding

BY B. VICTOR, D. F. FARSON, S. REAM, AND C. T. WALTERS

ABSTRACT

High-power, high-beam-quality fiber lasers can produce high depth/width aspect ratio welds at productive travel speeds with minimal distortion. However, autogenous laser welds made at high-power density often also have sharp toe angles and undercut at the weld toes. In this research, welds were made with a 10-kW IPG fiber laser and a multispectral zinc sulfide beam-shaping optic designed to direct a portion of the beam to the sides of the weld pool to increase melt spreading and smooth the weld toes in a single pass. Toe angles of stainless steel welds were improved using the beam-shaping optic and experimentally optimized parameters. Externally measured toe angles of welds made with a conventional focus optic were 125 deg, while those made with the custom optic were 163 deg.

Introduction

Lasers produce a coherent monochromatic beam of radiation that can be collimated and transmitted over relatively large distances and also focused to a small spot diameter (Ref. 1). Depending on the power density and motion of the focused beam on a material surface, welding, cutting, drilling, heat treating, and other materials-processing applications can be accomplished by lasers. In penetration welding (also referred to as keyhole welding), a beam is focused on a metal surface with sufficiently high power density to cause melting and evaporation. The vapor pressure then forms a cavity, or keyhole, which is traversed over the material surface material to form a keyhole weld (Ref. 2). Such welds have high aspect ratios and can be made at fast travel speeds, which makes them attractive for applications requiring precision, low heat input and high productivity. High-power, high-beam-quality, solid-state lasers such as the one used in this research are emerging as a significant advancement in laser welding. They offer unique capability to make high aspect ratio laser welds at fast travel speeds with low heat input.

Conduction-mode laser welding occurs when the focused power density is insufficient to cause significant vaporization at the work surface and thus does not generate a keyhole (Ref. 2). In this welding mode, laser energy is partially absorbed at the work surface and is transported into the underlying material by thermal conduction (Ref. 3) and melt convection (Ref. 4). The relatively slow rate of energy transport by these mechanisms, in comparison to welding travel speed, limits the weld penetration and aspect ratio. Both conduction- and keyhole-mode laser welding were investigated in this research.

Beam-shaping optics are designed to modify a laser beam to produce a desired spatial power distribution. In addition to materials processing, laser beam shaping is also used to produce a wide range of irradiance distributions for illumination, holography, lithography, printing, weaponry, and optical data/image processing (Refs. 5, 6). Both reflective and refractive beam-shaping optics can be designed to accommodate these different needs, and they can be further classified into aperturing, field mapping, and beam integration designs (Ref. 7).

Previous researchers have used custom optic configurations based on different beam-shaping methods to produce welds with desired characteristics and shapes. Killpatrick suggested the use of custom power distributions to weld dissimilar materials. Each material would be welded with one section of a split beam. Each section of the beam had a different irradiance to produce the desired melt volume in each material. He also suggested using a custom beam shape to control the heat-affected zone (HAZ) and permit stress relief as the fusion zone cools (Ref. 8). Liu and Kannatey-Asibu used an elliptical beam for preheat followed by a line source for welding. The elliptical beam was also used for post heating the weld (Ref. 9). In a separate study, Liu and Kannatey-Asibu used a dual beam (twin spot) configuration to weld with one spot and preheat or post-heat with the other (Ref. 10). Russ et al. welded aluminum with a double focus (twin spot) technique to reduce porosity and spatter (Ref. 11). Kell et al. used diffractive optical elements to change power distribution and therefore adjust the shape of weld penetration profiles (Ref. 12). Hammond et al. also used diffractive optical elements to produce a custom power distribution for joining dissimilar materials including combinations of aluminum, Inconel®, and stainless steel (Ref. 13).

Prior researchers have reported on a modified hybrid laser gas metal arc welding process that used a defocused laser spot to promote a wider weld pool than conventional gas metal arc welding (GMAW) (Refs. 14, 15). This defocused laser beam was positioned alongside the GMA weld to promote spreading of the weld pool and to improve the weld toe angle increasing fatigue life. Experimental and simulation studies of a similar modified hybrid laser arc welding process demonstrated that weld bead humping could be suppressed by using a defocused laser beam to increase weld bead width (Refs. 16, 17). Others have used oblong spots, twin spots, or other custom shapes to reduce weld pool humping at high speeds, decrease porosity, reduce defects from coated materials, alter the penetration profile, or improve weld quality (Refs. 18–20). However, the authors found no reports of prior work where beam-shaping optics were used to produce a deep penetration keyhole weld and then to smooth the weld surface in a single pass.

The goal of this research was to develop a custom optic for laser beam shap-

KEYWORDS

Fiber Lasers
High-Power Lasers
Keyhole Welding
Undercut
Toe Angle

B. VICTOR and S. REAM are with Edison Weding Institute, Columbus, Ohio. D. F. FARSON is with Welding Engineering Program, The Ohio State University, Columbus, Ohio. C. T. WALTERS is with Craig Walters Associates, Powell, Ohio.

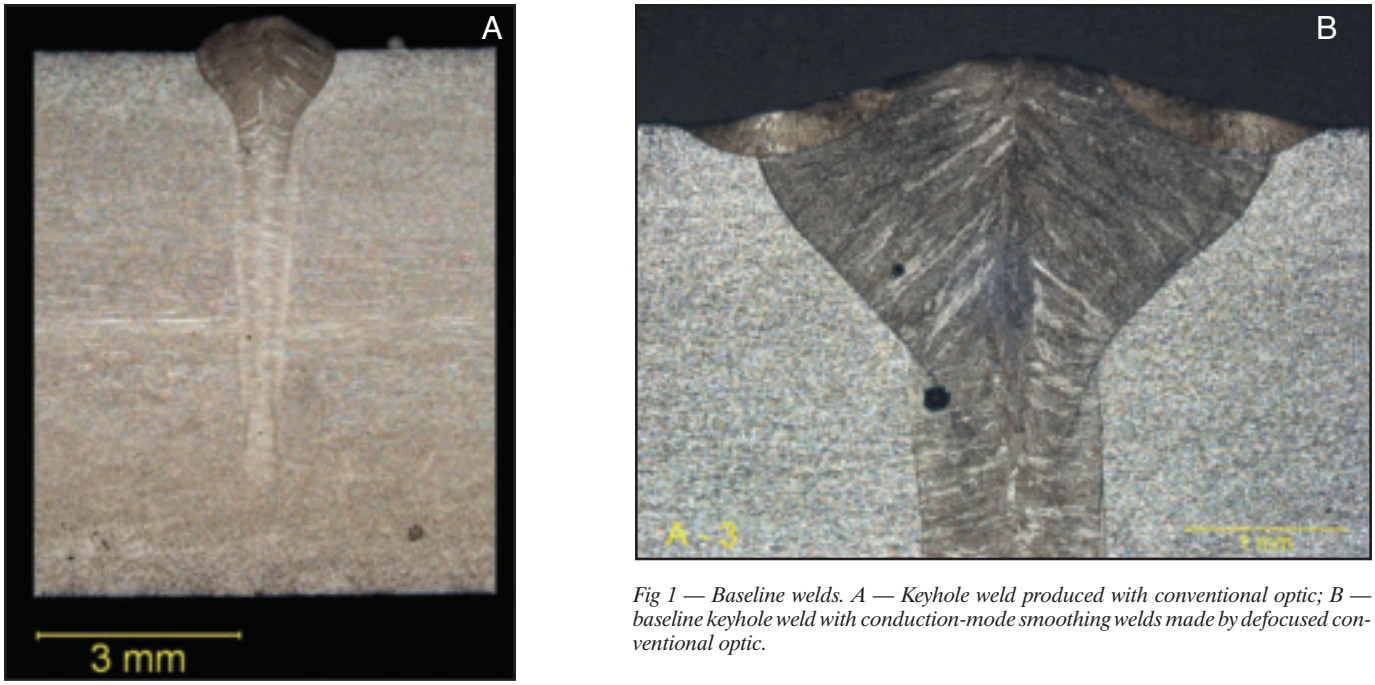

Fig 1 — Baseline welds. A — Keyhole weld produced with conventional optic; B — baseline keyhole weld with conduction-mode smoothing welds made by defocused conventional optic.

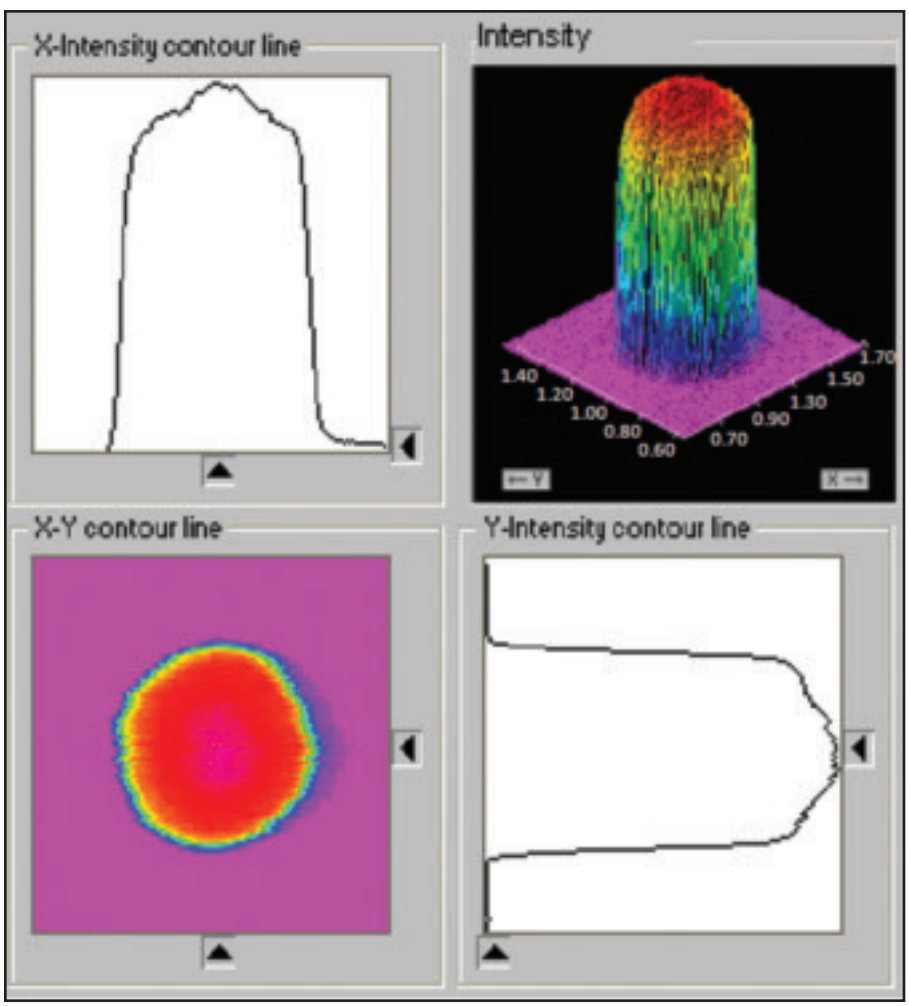

Fig. 2 — Qualitative laser beam intensity distribution plots for the 6.0-kW focused beam used for keyhole mode welding: (upper left) X-axis intensity plot, (upper right) color contour intensity plot, (lower left) color intensity plot, (lower right) Y-axis intensity plot. Dimensions are in mm.

ing and parameters for producing deep-penetration, high-aspect-ratio laser welds with remelted smooth toes in a single pass. The research focused on the following objectives: produce baseline welds with conventional optics to show typical fusion profile and weld toe geometry; design a custom three-spot optic solution capable of welding and smoothing the weld toes in a single pass to reduce geometric stress concentrations; produce welds with the custom three-spot optic; and compare the resulting weld profiles to cross sections from baseline welds produced with conventional optics.

Baseline Weld Trials

In the initial phase of the research, welding trials were conducted with conventional single-spot focusing optics and a 10-kW IPG Yb-fiber laser to produce typical weld profiles. The weld toes of baseline welds were also subsequently remelted and smoothed by two conduction-mode laser welds applied along the edges of baseline welds. The conventional-optic parameters for producing penetration and conduction welds were then used to develop the specifications for the custom beam-shaping optic.

Partial penetration keyhole welds were made in the bead-on-plate configuration in the flat position. The material for all welding trials was 8-mm-thick, Type 304 stainless steel. Argon shielding gas was supplied from a 10-mm off-axis shielding nozzle at a flow rate of 50 ft^3/h (23.6 L/min). Keyhole welds were produced using a conventional parabolic focusing optic with the minimum focus spot size of 500 μm located on the top surface of the

plate. Welds were made at all combinations of travel speeds of 120 in./min. (51 mm/s), 160 in./min (68 mm/s), and 200 in./min. (85 mm/s) and laser powers of 5 and 7 kW. From these trials, one set of parameters, listed in Table 1, was selected as the baseline condition for future comparisons. Figure 1A contains a photograph of a cross section taken from a weld bead produced with the baseline parameters.

Tests were completed to determine the relative power density and spot size necessary for conduction-mode laser-weld-smoothing of the toes of previously produced baseline keyhole welds. The laser power was reduced, and the focal position was raised, to produce an out-of-focus spot on the work surface. The beam was then traversed along the baseline weld toes to remelt only the top surface. The reduced power and out-of-focus spot size produced a low power density at the work surface, resulting in a conduction-mode weld. During optimization of conduction-mode welding parameters, travel speed and laser power were restricted to ensure that the developed weld-toe smoothing parameters could be implemented simultaneously with the main penetration parameters. In the final optical system implementation, the total laser power would be divided into three beams. The main beam would be focused to produce the keyhole-mode penetration weld, and the other two beams would trail the first beam to remelt and smooth the toes of the main weld bead. The total power of all three beams needed to be less than the 10-kW maximum power output of the fiber laser source. For this reason, the laser power for weld toe smoothing was restricted to less than 2 kW and the power of the main beam was equal to the baseline power of 6 kW.

The focal position, laser power, and lateral distance from the weld centerline were adjusted to develop the optimum weld toe smoothing parameters listed in Table 1. Figure 1B displays a photograph of a cross section of a baseline laser weld with weld toes smoothed by conduction-mode welds made at the optimum parameters.

With trials proving the feasibility of smoothing weld toes, the keyhole welding beam and the conduction smoothing beam were characterized to determine the constraints for the custom optic design. The power density and spot size of the main beam was measured using a focused laser beam diagnostic instrument (Focus Monitor, PRIMES GmbH). The results are displayed in Fig. 2. The power density and spot size of the smoothing beam was measured using a large-diameter laser beam diagnostic instrument (Beam Monitor, PRIMES GmbH) with results as displayed in Fig. 3. The $1/e^2$ focus spot diameter and peak power density measurements for the two beams are summarized in Table 2.

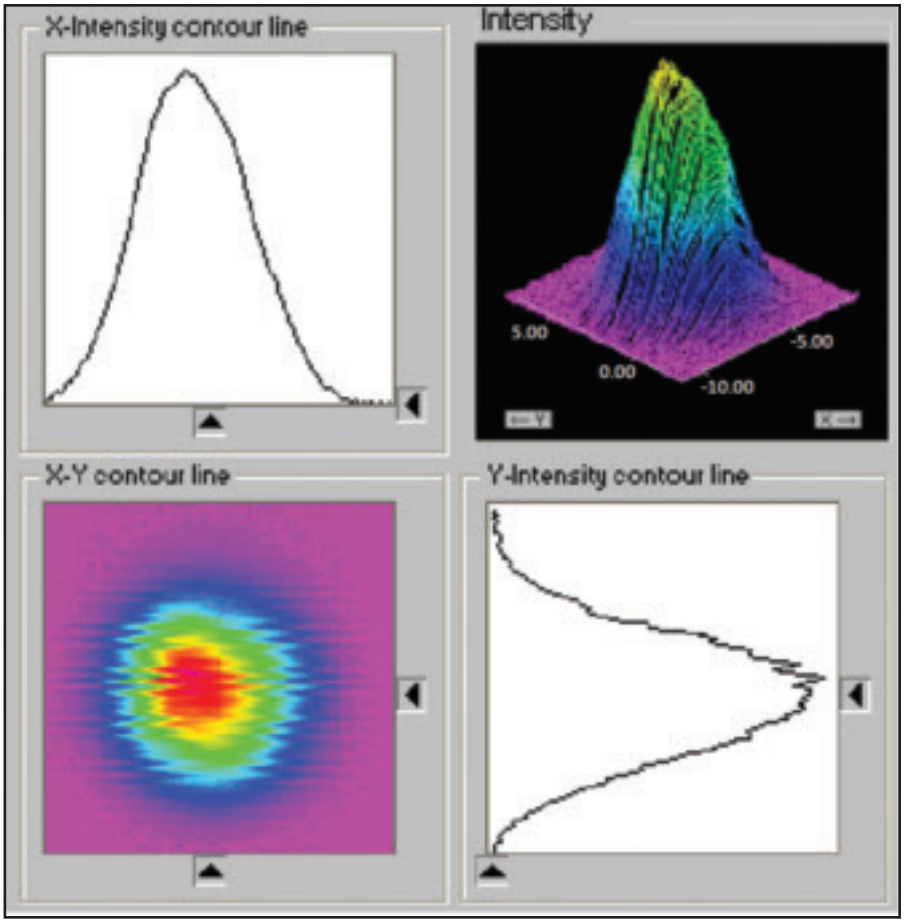

Fig. 3 — Qualitative laser beam intensity distribution plots of the 1.5-kW defocused beam used for conduction-mode toe smoothing welds: (upper left) X-axis intensity contour plot, (upper right) color contour intensity plot, (lower left) color intensity plot, (lower right) Y-axis intensity contour plot. Dimensions are in mm.

In addition to the spot size and power density of the main beam and smoothing beams, the relative locations of the beams were also needed to design the custom optic. The lateral (cross-seam) spacing of the two smoothing beams was determined from the width of the baseline weld. Determining the longitudinal (travel-direction) spacing between the main beam and

Table 1 — Baseline Parameters for Keyhole Welding with Conventional Parabolic Focusing Optics

Travel Speed (in./min)	Laser Power (kW)	Fiber Diameter (μm)	Collimation Lens Focal Length (mm)	Focusing Mirror Focal Length (mm)	Spot Size (μm)	Focal Position
120	6	300	150	250	500	work surface

Table 2 — Welding Parameters for Conduction-Mode Smoothing of Baseline Weld Toes Using Conventional Optics

Travel Speed (in./min)	Laser Power (kW)	Fiber Diameter (μm)	Collimation Distance (mm)	Focusing Distance (mm)	Focal Position (mm)	Distance from Centerline (mm)
120	1.5	300	150	250	+24	1.3

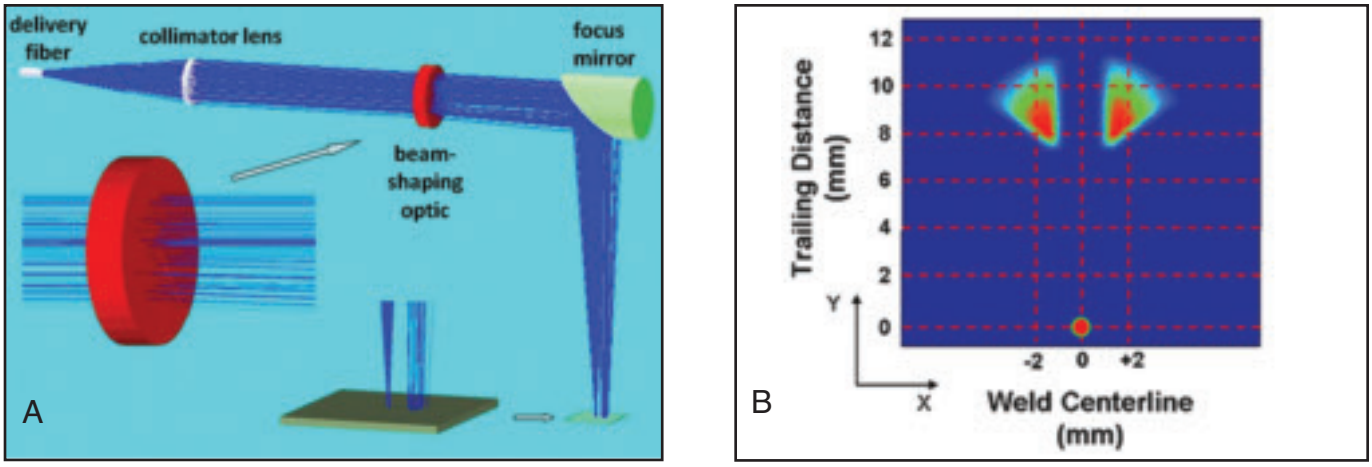

Fig. 4 — A — Ray-tracing model of laser beam propagation through the fiber laser beam delivery optics, including the beam-shaping optic; B — color plot of the power density distribution on the work surface predicted by ray tracing.

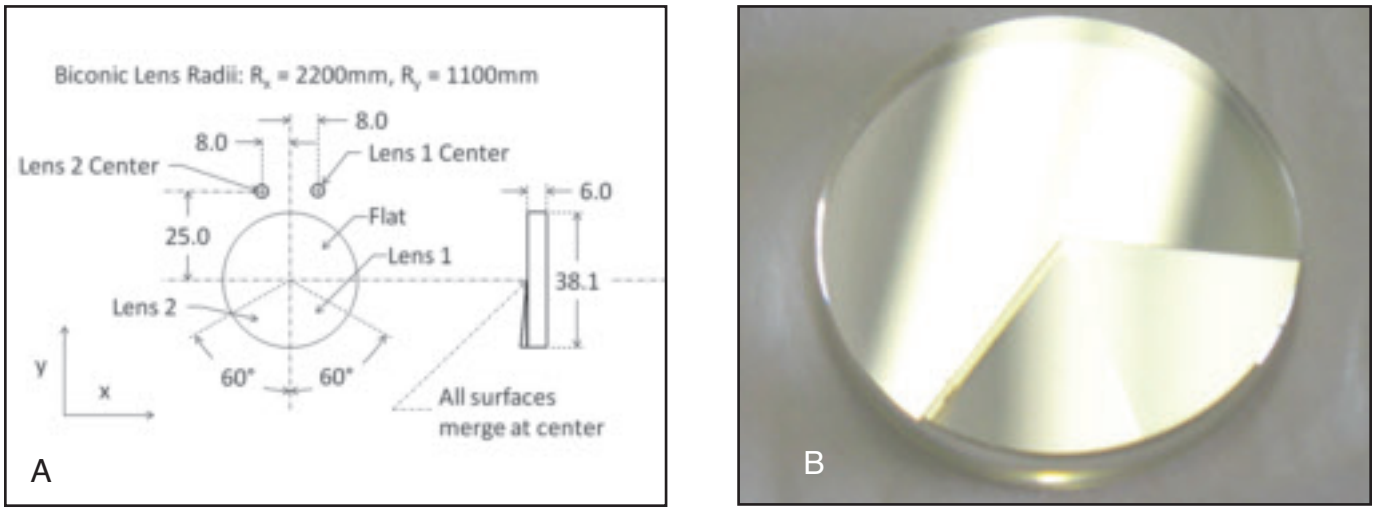

Fig. 5 — Three-spot beam-shaping optic. A —Design; B — finished optic. Dimensions are in mm.

Table 3 — Summary of Quantitative Beam Measurement Data for Main Beam and Smoothing Beam Intensity Profiles Illustrated in Fig. 3

Welding Beam	Spot Size (mm)	Power Density (kW/cm^2)
Main beam	0.498	3080.4000
Smoothing beam	6.198	4.9716

Table 4 — Target Design Specifications for the Power, Power Density, and Location of Each Beam of the Beam-Shaping Optic

Welding Beam	Power (kW)	Power Density (kW/cm^2)	Main/Smoothing Beam Power Ratio	Positive Relative to main beam X, Y (mm)
Main beam	6.0	3000	4	0, 0
Smoothing Beam 1	1.5	5	1	1, 10
Smoothing Beam 2	1.5	5	1	–1, 10

the smoothing beams was subjective. Because all of the preliminary proof-of-concept welding trials were produced with single-spot conventional optics, the main weld and surrounding base metal was relatively cool when the second and third smoothing passes were attempted. For the conduction beams of the custom optic to remelt and smooth the weld toes with the same effectiveness as the preliminary tests, the main weld needed to be solidified at the focus points of the smoothing beams. The longitudinal spacing from the main beam to the trailing beams was therefore determined as 10 mm by estimating the weld pool size and shape from the end crater produced during baseline welding tests with conventional optics. The final parameters for all three beams are listed in Table 3.

Beam-Shaping Optic Design

The custom beam-shaping optic was designed to be inserted into existing welding optics. To produce three spots, the single custom optic needed to have three optical surfaces with sharp transitions between them. The optic was designed to be diamond-machined from multispectral zinc sulfide (ZnS), a transmissive optical material prepared from standard zinc sulfide blanks by a hot isostatic pressing process. This material has desirable properties for near-infrared high-power laser applications including relatively low scat-

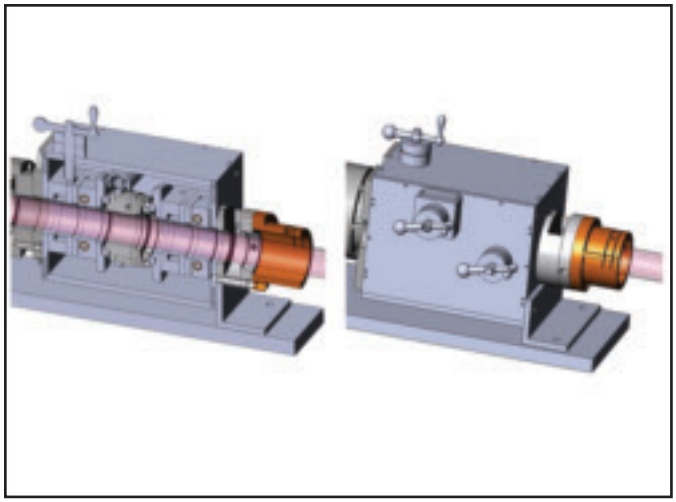

Fig. 6 — Beam-shaping optic mount with adjustment in three axes and water cooling.

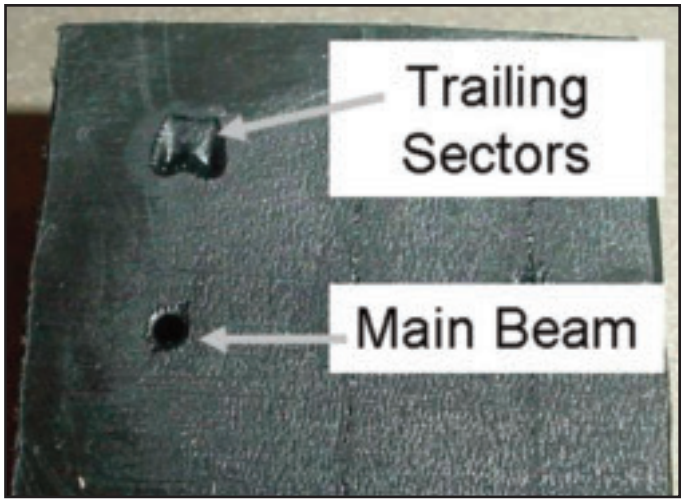

Fig. 7 — Photograph of burn pattern produced by the beam-shaping optic on black polyethylene.

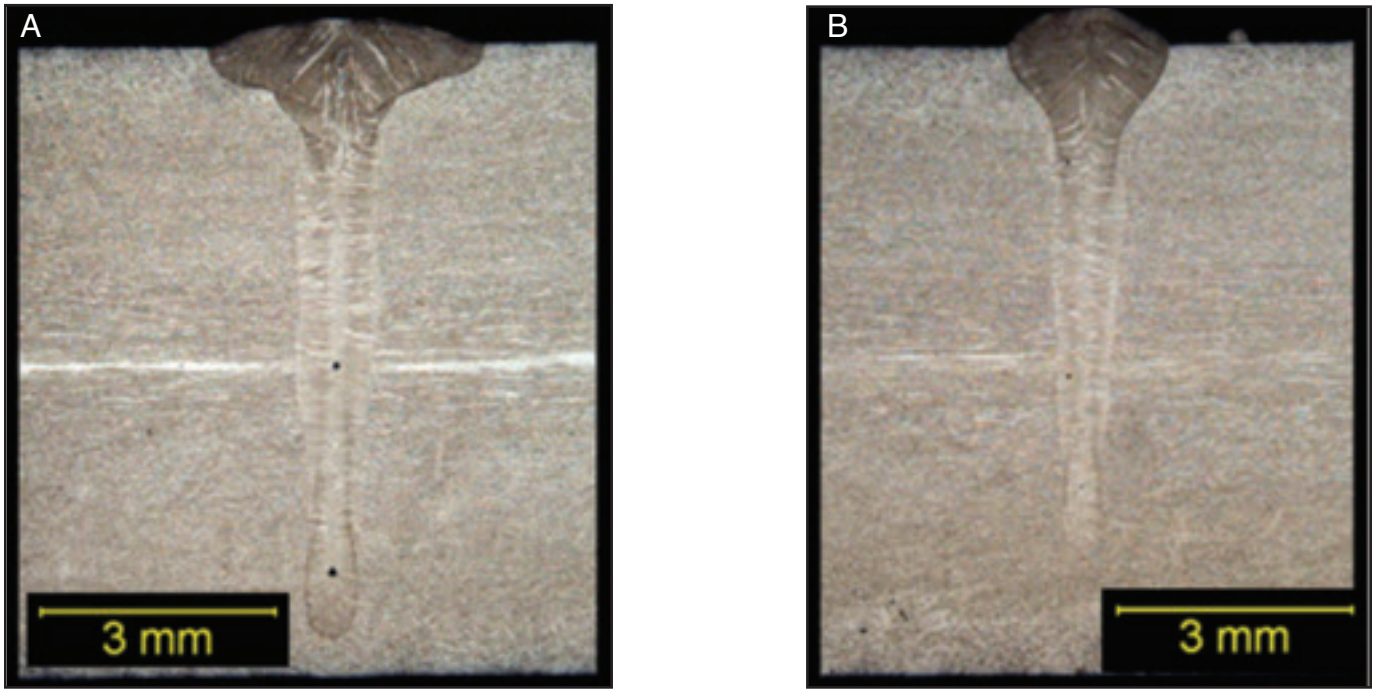

Fig. 8 — Comparison. A — Beam-shaping optic weld cross section; B — baseline weld cross section.

ter, high thermal conductivity, and good transmittance in the wavelength range from 0.4 to 12 microns (Ref. 21).

The beam-shaping optic was designed to fit into the collimated section of the current welding optics, illustrated in Fig. 4A. The collimating lens was a 150-mm plano-convex ZnS lens and the focusing mirror was a 90-deg 250-mm parabolic copper mirror. The beam-shaping optic was designed to produce a beam power density distribution similar to the experimentally determined specifications listed in Table 3. The optic was designed by Craig Walters Associates with the help of a ray tracing software program (ZEMAX, Zemax Development Corp.), which predicted beam propagation through the beam-delivery system and the power density distribution on the work surface. Iterative adjustments were made to an initial 3-sector beam-shaping optic design until the output power distribution on the work surface was approximately equal to that required by the design specifications. The image showing the final work surface power density distribution in Fig. 4B is discussed in more detail below.

The custom optic was designed as a 38-mm lens having a flat face on two thirds of the surface. This allowed 67% of the beam to travel through the custom optic unaltered. This 67% was then focused by the parabolic copper focusing mirror to become the main welding beam. The remaining 33% of the power was redirected by the two sector-shaped lenslets to become the two weld-smoothing spots after focusing by the copper mirror. The two

Fig. 9 — End craters of typical welds produced by the beam-shaping optic.

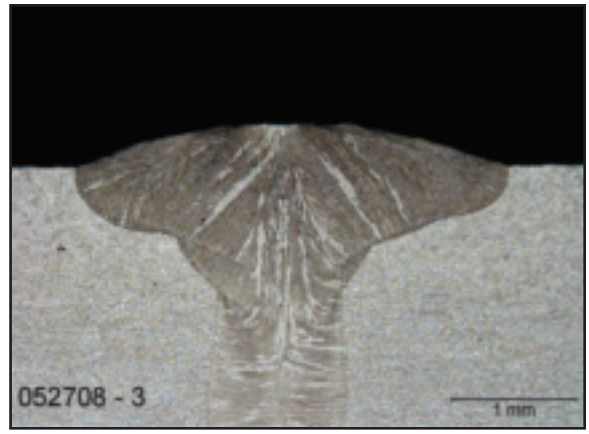

Fig. 10 — Cross section of a typical weld produced by the beam-shaping optic.

Table 4 — Target Design Specifications for the Power, Power Density, and Location of Each Beam of the Beam-Shaping Optic

Welding Beam	Power (kW)	Power Density (kW/cm^2)	Main/Smoothing Beam Power Ratio	Positive Relative to main beam X, Y (mm)
Main beam	6.0	3000	4	0, 0
Smoothing Beam 1	1.5	5	1	1, 10
Smoothing Beam 2	1.5	5	1	–1, 10

Table 5 — Beam-Shaping Optic Welding Parameters that Produced a Weld with Penetration Approximately Equal to the Baseline Weld at the Same Travel Speed

Travel Speed (in./min)	Laser Power (kW)	Fiber Diameter (μm)	Collimation Distance (mm)	Focusing Distance (mm)	Focal Point Elevation
120	10	300	150	250	Part Surface

Table 6 — Comparison of Weld Toe Angles of Welds

Baseline Weld Toe Angles Deg	Beam Shaping Optic Weld Toe Angles Deg
115	165
140	160
120	165
125	165
128	157
136	163
114	159
139	158
119	170
118	165
avg. 125	avg. 163

lenslets were tilted 60-deg sectors that separate 16.5% of the beam power from the main beam to form the two trailing beams. Each of these lenslets had a biconic curvature to further define the shape of the trailing focused spots. The trailing spots were designed to have a triangular shape at the welding plane rather than round spots to simplify machining complexity. The predicted power density distribution is shown in Fig. 4B. The (X,Y) locations of the peak intensities of the two trailing spots relative to the center of the main beam are 1.5 mm, 8.0 mm, and –1.5 mm, 8.0 mm, which are approximately equal to the design specifications.

The finalized design shown in Fig. 5A was manufactured from a ZnS blank. Using a fast-axis diamond machining system, the biconic lenslets were first cut and then the flat section was fly cut to define the sectors. A photograph of the resulting optic is shown in Fig. 5B. A final inspection of the machined optic showed that its surface geometry was reasonably close to the design geometry. Each of the two lens sectors was designed to have a biconic curvature of 2200 mm in the X axis and 1100 mm in the Y axis. After machining, the radii were measured to be 2201 mm in the X axis and 1099 mm in the Y axis. Each of the sectors was to occupy 60 deg of the total optic. However, the final dimensions of the sectors were machined as 55 and 64 deg due to machining errors. These minor differences were not expected to affect the performance of in-process weld toe smoothing.

Beam-Shaping Optic Alignment, Characterization, and Welding

An alignment mechanism was built to allow the custom optic to be installed in the beam-delivery system between the collimating lens and the focusing mirror as illustrated in Fig. 4A. After installation, the optic was aligned and laser power measurements were taken to test the power loss through the custom optic. Welding trials were conducted and then compared to welds produced by conventional optics.

The asymmetric beam-shaping optic had to be precisely aligned to the collimated input beam in two translational directions parallel to the plane of the optic surface and in the rotational axis normal to the optic surface. Translation of the optic in the X axis (Fig. 5A) adjusted the power ratio between the two trailing sectors. Translation of the optic in the Y axis adjusted the power ratio between the main beam and the trailing sectors. Rotational adjustment of the optic controlled the angle between the Y-axis (defined in Fig. 4B) of the power distribution on the work surface and the welding travel direction. In addition to providing precision alignment relative to the input beam, the optic mount was also water-cooled to accommodate continuous operation at 10 kW. Figure 6 illustrates the optic mount de-

signed by EWI.

The beam-shaping optic was installed, aligned, and optically characterized. The output power of the entire optical beam-delivery system was measured at the work with continuous wave input beam powers ranging from 1 to 10 kW. The beam-shaping optic caused an average of 2.1% power loss compared to the output power of the system without the optic. Since the optic had an antireflective coating to reduce reflectance losses to well less than 1%, the power attenuation is presumed to be primarily due to a combination of absorption and forward scatter. Multispectral ZnS is a polycrystalline material. Due to the crystalline structure, forward scatter can attenuate 1μm-wavelength laser beam power by as much as 1–2%. To verify its capability to operate at high transmitted power without damage, the optical system was tested at 10 kW for one minute with no apparent change in the optical pattern, focus spot diameters or thermal damage to the optic.

The power density distribution on the work surface was qualitatively imaged by thermal burn patterns. This approach was adopted because the size and complexity of the pattern generated by the beam-shaping optic could not be characterized with available beam diagnostic instruments. Low-power burn patterns were made on laser burn paper (ZAP-IT paper, Zap-It Corp.) to verify the focused pattern and determine optimum focus location. The focal distance that provided the minimum main beam spot size was determined to be equal to 250 mm, the focal length of the parabolic focusing mirror. The paper burns also verified that the beam-shaping optic produced a spatial power distribution that was qualitatively similar to the ray-tracing simulations.

To observe the relative spacing and power density of the three spots at higher power, burn patterns were made on black polyethylene. When a high-power, short pulse was focused onto the black plastic surface, some of the plastic was ablated and the remaining depressions gave an indication of the locations and power distribution of the three spots. Figure 7 shows an example of such a test burn on the surface of black polyethylene.

To adjust the alignment of the optic, multiple polyethylene burn test were conducted and each axis was incrementally adjusted between shots in increments of motion of 1 mm in the X and Y axes and 2.25-deg increments in the rotational axis. From the burn spots, it was observed that the trailing sectors overlapped rather than being separated by about 1 mm as designed. Also, this trailing shape was only 6 mm behind the main beam rather than the designed 10 mm. The optical assembly was moved vertically from the work surface in 1-mm increments and burn patterns were analyzed to investigate the variation of laser power density distribution with focal distance changes.

When the focal distance was increased by 4 to 254 mm, the trailing sector distributions still overlapped but the distance between the main beam and the trailing sectors increased to 8 mm. Changes in focal distance beyond +/- 4 mm above or below the optimum of 250 mm altered the shape of the main beam, indicating that welding at distances more than 4 mm from the optimum focus of the main beam would decrease weld penetration. Since the increase in distance between the main spot and the trailing spots was minimal, the best focal position for welding was determined to be at a distance of 250 mm from the parabolic focusing mirror. With the best alignment determined from burn tests, welding trials were conducted with the custom three-spot optic.

Partial penetration welds were completed using the beam-shaping optic on 8-mm 304 stainless steel in the bead-on-plate configuration with off-axis shielding provided by argon gas flowing at 50 ft^3/h from a 10-mm nozzle. In the conventional optic trials, the best parameters were determined as 6 kW of laser power in the main beam at a travel speed of 120 in./min. Beam-shaping optic welding trials were conducted at 120 in./min travel speed with 9 kW of laser power, which also produced 6 kW of power in the main beam. In addition to replicating the baseline welding power and travel speed, a full matrix of combinations of total laser powers of 8, 9, and 10 kW and travel speeds of 120, 160, and 200 in./min were tested.

Results from the welding trials showed that the power distribution produced by the beam-shaping optic was successful in producing smoother weld profiles than a single beam focus with conventional optics, although the actual weld pool shapes were different than intended. The beam-shaping optic was designed to produce a main keyhole-mode weld pool and two trailing conduction-mode weld pools at the toes of the solidification of the main pool. Instead, the main weld pool was still liquid at the trailing focus spots locations so the optic produced one weld pool rather than the proposed three. This difference was attributed to an increased interpass temperature at the trailing spot locations and to the shorter-than-designed spacing of the trailing sectors from the main beam.

All weld tests showed similar penetration, reduced bead convexity, and improved, larger weld toe angles compared to the baseline weld. The optimum welding parameters shown in Table 4 were selected from the test matrix as those which produced a penetration approximately equal to the baseline weld at the same travel speed. Figure 8 compares the cross sections of welds produced using the conventional optic weld and the beam-shaping optic weld. The cross sections are seen to be similar.

Figure 9 displays a photograph of representative weld end craters produced during the custom optic welding trials. It appears that the beam-shaping optic power distribution produced a weld pool with two distinct melt zones corresponding to the main beam and the two trailing beams. However, these two zones were part of the same continuous weld pool. The extra heat provided by the trailing beam shape increased the weld pool width, which increased the toe angles of the weld bead. Figure 10 shows a magnified cross section of the weld produced by the custom optic. The fusion zone profile clearly shows that the power density distribution produced a relatively shallow conduction-mode melt zone superimposed on a deep penetration keyhole weld.

The toe angles of weld beads produced by the conventional optic and the beam-shaping optic were measured with image analysis software (Image-Pro®, Media Cybernetics, Inc.) and are listed in Table 5. A single focus spot produced weld beads with average toe angle of 125 deg, while the beam-shaping optic produced weld beads with average weld toe angle of 163 deg. Since the entire width of the weld was molten during the welding process, the profile of the top surface of the weld bead cross section was approximately spherical. This is qualitatively similar to previously-reported results for arc spot weld deposit profiles (Ref. 14).

Conclusions

A transmissive zinc sulfide optic was designed to produce a power distribution at the work surface that would result in smoother weld bead profiles. The baseline welds produced using conventional optics were convex with an average weld toe angle of 125 deg. The actual power distribution of the designed beam-shaping optic had one main penetration beam containing approximately 67% of the total input laser power and two trailing focus intensity distributions that overlapped significantly. In spite of the differences between the desired intensity distribution and the actual distribution, welds produced with the custom optic showed an improvement in weld toe angle from an average of 125 deg to an average of 163 deg.

References

1. Kielhorn, W. H. 1991. *Welding Handbook*, Vol. 1, Welding Science and Technology. Ch. 22. 7th edition, American Welding Soci-

ety. Miami, Fla.
2. Steen, W. 2003. *Laser Material Processing.* 3rd edition., Ch. 4. Springer, New York, N.Y.
3. Ready, J. F., and Farson, D. F. 2001. *LIA Handbook of Laser Material Processing*, 1st edition., Ch. 4. Laser Institute of America, Orlando, Fla.
4. Cho, J. H., and Farson, D. F., Milewski, J. O., and Hollis, K. J. 2009. Weld pool flows during initial stages of keyhole formation in laser welding. *J. Phys. D:Applied Phys*. 42(17): 175502.
5. Shealy, D. 2002. Historical perspective of laser beam shaping. *Proc. SPIE* 4770: 28–47.
6. Dickey, F., Weichman, L., and Shagam, R. 2000. Laser beam shaping techniques. *Proc. SPIE* 4065: 338–348.
7. Webb, C., and Jones, J. 2004. *Handbook of Laser Technology and Applications*. Vol. 2, Pt. C, Ch. 4, p. 1442.
8. Killpatrick, D. 1993. Laser beam shaping takes the next step. *Industrial Laser Review* 8(7): 18.
9. Liu, Y. N., and Kannatey-Asibu, E. 1998. Finite element analysis of heat flow in dual-beam laser welded tailored blanks. *J. Manuf. Sci. Eng.-Trans*. *ASME* 120(2): 272–278.
10. Liu, Y. N., and Kannatey-Asibu, E. 1997. Experimental study of dual-beam laser welding of AISI 4140 steel. *Welding Journa,* 76(9): 342-s to 348-s.
11. Russ, A., Gref, W., Leimser, M., Dausinger, F., and Hugel, H. 2002. Double focus technique — influence of focal distance on the welding process. *Proc. SPIE* 5121: 362–368.
12. Kell, J., Tyrer, J., Higginson, R., Thomson, R., Jones, J., and Noden, S. 2006. Holographic diffractive optical elements allow improvements in conduction laser welding of steels. *Proceedings of the International Conference on the Applications of Lasers and Electro-Optics ICALEO 2006*, Scottsdale, Ariz., pp. 8–17.
13. Hammond, J., Johnson, E., Koehler, C., Stack, J., and Suleski, T. 1999. Diffractive optics for laser welding and bonding. *Proc. SPIE* 3633: 206–213.
14. Cho, M. H., Farson, D., Lim, Y. C., and Choi, H. W. 2007. Hybrid laser/arc welding process for controlling bead profile. *Sci. Technol. Weld. Join*. 12(8): 677–688.
15. Lim, Y. C., Farson, D. F., Cho, M. H., and Cho, J. H. 2009. Stationary GMAW-P weld metal deposit spreading. *Sci. Technol. Weld. Join*. 14(7): 626–635.
16. Choi, H. W., Farson, D., and Cho, M. H. 2006. Using a hybrid laser plus GMAW process for controlling the bead humping defect. *Welding Journal* 85(8): 174–179.
17. Cho, M. H., and Farson, D. 2007. Simulation study of a hybrid process for the prevention of weld bead hump formation. *Welding Journal* 86(9): 253–262.
18. Mombo-Caristan, J., Mueller, R., Sharp, C., and McCay, M. 1997. Parabolic mirror adapted-alignment for high speed-high power laser welding with an oblong focused beam spot. *Proceedings of the International Conference on the Applications of Lasers and Electro-Optics ICALEO — Section G*. pp. 191–199.
19. Banas, C. 1986. High power laser welding. *The Industrial Laser Annual Handbook*. Pennwell Books.
20. Hsu, R., Fliss, S., and Heinemann, S. 1999. High power CO_2 laser aluminum tailored blank welding. *International Body Engineering Conference & Exposition*, Session: tailor welded blanks, Paper Number: 1999-01-3165, Detroit, Mich.
21. II-VI, Inc. 2009. Zinc Sulfide Multi-Spectral (ZnS MS) *http://www.iviinfrared.com/zinc_sulfide_multispectral_znsms,* accessed Feb. 8.

Preparation of Manuscripts for Submission to the *Welding Journal* Research Supplement

All authors should address themselves to the following questions when writing papers for submission to the Welding Research Supplement:

- Why was the work done?
- What was done?
- What was found?
- What is the significance of your results?
- What are your most important conclusions?

With those questions in mind, most authors can logically organize their material along the following lines, using suitable headings and subheadings to divide the paper.

1) **Abstract.** A concise summary of the major elements of the presentation, not exceeding 200 words, to help the reader decide if the information is for him or her.

2) **Introduction.** A short statement giving relevant background, purpose, and scope to help orient the reader. Do not duplicate the abstract.

3) **Experimental Procedure, Materials, Equipment.**

4) **Results, Discussion.** The facts or data obtained and their evaluation.

5) **Conclusion.** An evaluation and interpretation of your results. Most often, this is what the readers remember.

6) **Acknowledgment, References and Appendix.**

Keep in mind that proper use of terms, abbreviations, and symbols are important considerations in processing a manuscript for publication. For welding terminology, the *Welding Journal* adheres to AWS A3.0:2010, *Standard Welding Terms and Definitions.*

Papers submitted for consideration in the Welding Research Supplement are required to undergo Peer Review before acceptance for publication. Submit an original and one copy (double-spaced, with 1-in. margins on 8 ½ x 11-in. or A4 paper) of the manuscript. A manuscript submission form should accompany the manuscript.

Tables and figures should be separate from the manuscript copy and only high-quality figures will be published. Figures can be submitted as original line art or glossy photos or electronically as JPEGs/TIFFs at 300 dpi photos. To receive complete instructions and the manuscript submission form, please contact the Peer Review Coordinator, Erin Adams, at (305) 443-9353, ext. 275; FAX 305-443-7404. To get instructions and submit your paper online go to www.editorialmanager.com/wj.